Int. J. Heat Mass Transfer. Vol. 15, pp. 2353–2369. Pergamon Press 1972. Printed in Great Britain

THE TRANSPIRED TURBULENT BOUNDARY LAYER IN AN ADVERSE PRESSURE GRADIENT

J. DOUGLAS McLEAN and GEORGE L. MELLOR

Department of Aerospace and Mechanical Sciences,
James Forrestal Campus, Princeton University, Princeton, New Jersey, U.S.A.

(*Received* 24 *September* 1971 *and in revised form* 15 *February* 1972)

Abstract—An experimental program was carried out to study the effect of transpiration on a turbulent boundary layer in an adverse pressure gradient. A wind tunnel with a porous test wall was designed so that the blowing velocity and the strength of the pressure gradient could be varied in the course of the experiments. The effect of transpiration on the location of the separation point was observed. Measurements of mean velocity profiles and heat transfer rates were compared with predictions of a boundary layer calculation method based on an effective viscosity model. Predictions of skin friction were satisfactory, but there was noticeable error in the predicted velocity profile shapes near separation. It was also found that a form of the law of the wake provides a good representation of velocity profiles with blowing and could be used as the basis for an integral method of prediction.

NOMENCLATURE

C_f, skin friction coefficient, $\tau_w/(\frac{1}{2}\rho U^2)$;
D, constant in the law of the wall, 4·9;
H, velocity profile shape factor, δ^*/θ;
p, pressure;
R_θ, Reynolds number based on θ, $U\theta/\nu$;
T, temperature;
T_c, temperature of air in chambers behind porous wall;
T_w, temperature of porous wall;
u, mean velocity in the X direction;
u^+, u/u_τ;
u_τ, friction velocity, $(\tau_w/\rho)^{\frac{1}{2}}$;
U, freestream velocity;
U_{max}, freestream velocity in the constant pressure section;
v, velocity in the y direction;
W, wake function or experimental wake component;
X, streamwise coordinate;
y, vertical coordinate;
y^+, yu_τ/ν;
z, transverse coordinate;
α, pressure gradient parameter $\nu(dp/dx)/\rho u_\tau^3$;
δ, boundary layer thickness;
δ^*, displacement thickness;
δ', integral thickness for cases with blowing;
θ, momentum thickness;
κ, von Karman constant in the law of the wall, 0·41;
ν, kinematic viscosity;
π, strength of the wake component;
ρ, density;
τ, shear stress.

Subscripts and superscripts

w, value at wall;
∞, freestream;
0, value at beginning of pressure gradient;
$'$, instantaneous value of fluctuating part.

Other symbols

$\langle\ \rangle$, indicates time average.

INTRODUCTION

THE TURBULENT boundary layer with transpiration has become a matter of considerable practical interest in recent years because transpiration can be used very effectively to cool surfaces exposed to hot gas flows. The effectiveness of transpiration cooling is two-fold: heat is convected from the surface by the transpired fluid, and transpiration reduces the heat transfer coefficient of the external boundary layer, thereby reducing the amount of heat which would otherwise have to be convected from the surface. As a result, a small mass flow of cooling fluid can maintain a wall temperature very close to the initial temperature of the coolant.

In order to extend boundary layer prediction methods to include transpiration, it has been necessary to accumulate a store of empirical data detailing the effects of transpiration on turbulent boundary layer development under various conditions. In the case of planar, incompressible flow, the boundary conditions of primary interest are the streamwise pressure gradient and the distributions of blowing velocity and wall temperature. Early experimental investigations of transpiration concentrated on the case of constant pressure and constant blowing velocity, as in the measurements of Black and Sarnecki [1], Stevenson [2], McQuaid [3], Simpson *et al.* [4], and others. Simpson [4] and Whitten *et al.* [5] have presented mean velocity profiles and heat transfer measurements for cases of non-constant blowing velocity and wall temperature. Data such as these have led to the modification of the standard law of the wall to include the effects of blowing. Essentially equivalent formulations of the law of the wall with blowing have been proposed by Black and Sarnecki [1], Simpson *et al.* [4], and Stevenson [6].

For cases of slowly varying blowing velocity, Simpson [4] and Stevenson [7] have modified the velocity defect law for constant pressure to include the effects of blowing. Recently, cases with favorable pressure gradients have been investigated at Stanford, as in the studies by Loyd *et al.* [8] and Kearny *et al.* [9].

The aim of this investigation is to provide data in the case of a strong adverse pressure gradient leading to separation. Because in some of the applications of transpiration (the suction side of a turbine blade, for example) boundary layer separation imposes severe design limitations, the ability to predict the detrimental effect of transpiration on the separating boundary layer is important.

A feature of many of the adverse pressure gradient flows occurring in practice is that they involve very rapid deceleration of the freestream. That is, the pressure gradient is strong enough to bring the flow to separation within a relatively short streamwise distance from the start of the pressure gradient. It is known that the suddeness with which a flow is brought to separation affects the ultimate pressure recovery which can be achieved. For this reason it was decided that the effect of pressure gradient steepness should be investigated along with the effect of transpiration. The experiments were thus designed to include two different free-stream velocity distributions. Several transpiration rates were used with each of these distributions. One of the free-stream velocity distributions featured a relatively moderate adverse pressure gradient, while the other involved a pressure gradient stronger than any for which extensive mean velocity profiles had previously been reported in the literature. Thus this strong pressure gradient case, even without blowing, is an interesting flow in its own right. Two cases at constant pressure were also included in the experimental program.

EXPERIMENTAL APPARATUS

A general view of the wind tunnel developed for these experiments is shown in Fig. 1. The tunnel is of the open-return, suction type and is powered by a 50 hp variable pitch fan. The entire top wall of the tunnel is flat from the inlet screens to the diffuser, and the tunnel is of constant width. This geometry leads to nearly two-dimensional flow everywhere near the flat

top wall. Comments on the quality of this two-dimensionality will be made later in this section. The porous test wall comprises a 5 ft long section of the flat top wall, as shown in the drawing.

gradient. The forward section of the bottom wall is bolted in position with slotted brackets, allowing small adjustments of the pressure distribution in the section where the initial test boundary layer develops.

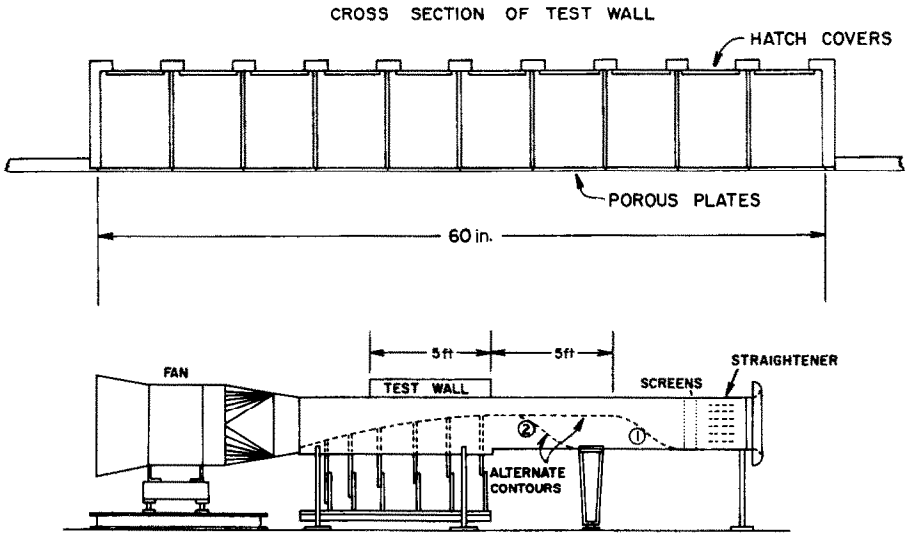

FIG. 1. Schematic view of the wind tunnel and the porous test wall.

The entry of the tunnel contains two sections of honeycomb flow straightener. The first section is 3 in. thick and is of $\frac{3}{8}$ in. cell size. The second section is a rectangular honeycomb of 1 in. cell size and is 12 in. thick. The straighteners are followed in the downstream direction by two layers of 18 mesh screen. The flow downstream of the screens was found to be parallel and quite steady. The remainder of the tunnel is in the form of a channel, rectangular in cross-section and 30 in. wide, with a variable bottom wall contour. The aft section of the bottom wall is flexible and is held in position by six motorized jacks, allowing easy adjustment of the pressure distribution on the test wall. The flexible section can be adjusted to give any distribution from constant pressure to a strong adverse pressure

Two different bottom walls can alternately be mounted in this section, with contours as shown in Fig. 1. Each contour results in a considerably different initial boundary layer on the test wall. Contour #1 immediately accelerates the flow and then maintains a constant free-stream velocity of 155 ft/s for a distance of about 5 ft. This condition leads to an initial test wall boundary layer with a displacement thickness of 0·170 in. Contour #2 keeps the flow at low velocity for a longer distance before accelerating it into a short section at 155 ft/s. This results in an initial displacement thickness of 0·065 in. Hereafter, these two conditions will be referred to as "thick boundary layer" and "thin boundary layer", respectively.

In order to prevent separation on the curved,

flexible portion of the bottom wall during the adverse pressure gradient tests, the bottom wall in this section contained a series of slots. These slots were open to the outside and were shaped so that air drawn in from the outside formed wall jets in the same way that a wall jet is formed on the suction side of a slotted wing flap. Separation on each of the side walls was prevented by an array of four small circular jets blowing tangent to the wall. These jets were of $\frac{1}{8}$ in. dia. and were supplied with air at high enough pressure to result in sonic flow at the jet exits. The momentum added by the jets was sufficient to prevent separation of the side wall boundary layers, but the mass flow added was so small that no noticeable displacement effect was produced.

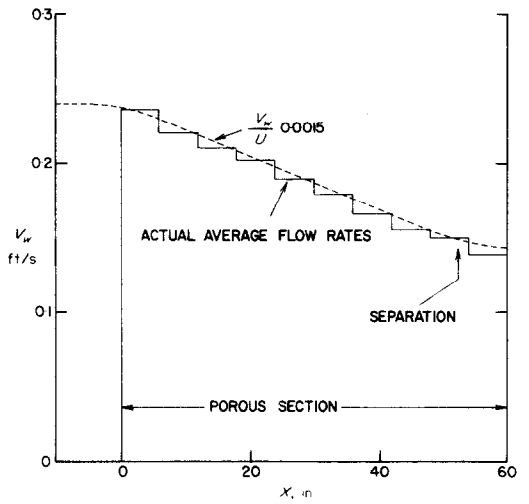

FIG. 2. Typical blowing velocity distribution.

The porous test wall was divided into ten separate sections so that the streamwise distribution of blowing rate could be controlled in a step-wise fashion, as shown in Fig. 2. The porous metal test wall panels were provided with a backing consisting of packs (15–30 sheets) of filter paper. At the flow rates used in these experiments, these packs provided a high enough pressure drop that the pressure gradient in the tunnel flow could not distort the blowing rate distribution significantly. With no flow in the tunnel, the entire wall was surveyed thoroughly with a 1 in. dia. mass flow probe, and the blowing velocity was found to be uniform to within ± 6 per cent. The porous metal panels were $\frac{1}{8}$ in. thick sheets of woven stainless steel Rigimesh surfaced on the flow side with a fine screen of the same type made up of wires of 0·0028 in. dia. At the upstream end of the porous wall, the screen mesh resulted in a roughness Reynolds number of about 10 in the worst case, the worst case being that of the thin initial boundary layer without blowing. Locations farther downstream, especially in the adverse pressure gradient cases, were characterized by lower values of roughness Reynolds number. Static pressure taps were provided in the joints between the wall sections.

Measurements

The locations of separation points in the pressure gradient experiments were determined by a simple visual technique. Small, pivoted metal vanes were traversed along the wall in such a way that they indicated whether the region near the wall was experiencing backflow for an appreciable portion of the time. A detailed interpretation of the response of these vanes to the flow field is given in [10]. The visually located separation points coincided closely with the points beyond which a prescribed pressure gradient could no longer be maintained. Three vanes were used in all of the separation experiments: one on the tunnel centerline and one 6 in. to each side of the centerline. Separation point locations given by the three vanes were always in agreement with each other.

Mean velocity measurements were made by means of a small pitot tube and a small static pressure tube which were traversed in combination. The tubes were mounted so that the pitot tube tip and the static tube holes were at the same axial location in the tunnel and were separated by 1 in. in the y direction. The pitot tube had a flattened opening 0·005 in. high by 0·05 in. wide and the static tube was 0·09 in. in

diameter with four 0·034 in. dia. static holes 1·0 in. back from the tip. Because of the complexity of the porous wall structure and the necessity of having a movable, flexible bottom wall, the method of traversing the probe combination was unorthodox. The probe combination was mounted on a tripod which held the pitot tube tip at a constant distance y from the test wall. This assembly was held against the wall by a strut mounted on a traversing carriage which ran on tracks in the side walls. Tests carried out with the aid of a telescope mounted on a micrometer traverse determined that the tripod assembly was capable of maintaining a constant distance y to within 0·001 in. The carriage was traversed in the streamwise direction so that the probe combination traced a history of the mean velocity $u(x)$ at constant y. The results of about 25 runs with the probe set at different values of y were required to assemble a conventional set of mean velocity profiles, $u(y)$ at constant x.

The effects of turbulence on the response of the probes were judged to be small. When known corrections for these effects were applied, it was found that the corrections changed the shapes of the velocity profiles so little that the conclusions drawn from the profiles would not have changed. Because these corrections were small and, at best, uncertain, the data reported here were left uncorrected. The variation of static pressure through the layer also had an effect on the readings of the probes. Using the data of Schubauer and Klebanoff [11] to estimate the variation of the static pressure, this effect was also found to be quite small. The mean flow yaw and pitch angles encountered by the probes were nowhere large enough to result in a significant error in the reading of either probe.

Experimental values of the skin friction coefficient were inferred from the mean velocity profiles by comparing the inner regions of the profiles with the appropriate law of the wall. In the absence of turbulent shear stress measurements, this was the only method available, because the skin friction in adverse pressure gradient flows rapidly becomes too small to be determined accurately by momentum considerations, and a Preston tube would require calibration in a pipe flow, which is difficult with blowing. For the cases without blowing, the standard logarithmic expression was used:

$$u^+ = \frac{1}{\kappa} \ln y^+ + D, \tag{1}$$

with $\kappa = 0{\cdot}41$ and $D = 4{\cdot}9$. For the cases with blowing, the form given by Stevenson,

$$\frac{2}{v_w^+}(1 + v_w^+ u^+)^{\frac{1}{2}} - 1 = \frac{1}{\kappa} \ln y^+ + D, \tag{2}$$

was used, although there is still an unsettled question† regarding the proper choice of D. Proposals have been made by several investigators concerning the variation of D with v_w^+. In order to check whether this matter would be of importance in the interpretation of our data, experimental values of C_f were determined using equation (2) with the values of D proposed by Stevenson [6] and those implied by the formula of Simpson [4]. Although the differences between the two determinations were not negligible,‡ the differences did not alter the

† Equation (2) is the result of integrating the simplified equation of motion valid near the wall, equation (4), with the assumption of a mixing length proportional to y outside the viscous sublayer. D is a function of v_w^+ and depends on the assumptions made concerning the integration through the viscous sublayer. The forms of equation (2) proposed by Black and Sarnecki [1] and Simpson [4] are results of two such different assumptions, and in both cases variations of D with v_w^+ are implied. Simpson presented a considerable amount of experimental data to support his particular choice. Stevenson, on the basis of more limited data, concluded that D is nearly constant at the no-blowing value. This question has not been settled to the satisfaction of the authors. The experiments reported here cannot throw light on this particular issue because adverse pressure gradient flows are ill-suited to careful investigations of the skin friction.

‡ Referring to Fig. 7, the values of C_f determined using Simpson's form of equation (2) were everywhere higher than those determined using Stevenson's form, shown by the symbols in the figure. The largest differences (about 0·0005 C_f units) were observed immediately downstream of the start of the porous section, where the C_f values according to Simpson were farther above the eddy viscosity predictions (curves) than the values according to Stevenson were below the curves. Approaching separation, the differences decreased until, at separation, the differences were smaller than the symbols in the figures.

conclusions drawn from the data with regard to the accuracy of the effective viscosity prediction method or the validity of the law of the wake. Because the differences were not important in this respect, and Stevenson's expression, D = constant, is the simplest, the C_f values presented in later sections are those obtained by comparison with Stevenson's expression. The validity of the law of the wall in any form in the presence of strong pressure gradients is discussed in a following section in connection with the predictions of the eddy viscosity theory.

The reported experimental values of the integral parameters δ^* and θ were obtained by integrating the appropriate law of the wall to the first data point and then integrating the data by the trapezoidal rule.

The porous wall and the injection air chambers behind the wall were instrumented with thermocouples to measure the temperatures required to calculate the heat transfer rate. In the case where all the variables are steady in time, a heat balance equation gives the heat transfer in terms of the Stanton Number:

$$St = \frac{v_w}{U_\infty}\left[\frac{T_w - T_c}{T_w - T_\infty}\right]. \qquad (3)$$

In this equation it has been assumed that the temperature of the air emerging from the porous surface is the same as the wall temperature. Because the thermocouples used to measure the wall temperature were mounted on the back surface of the porous wall, it also has to be assumed that the temperature of the porous wall was constant throughout its thickness. It can be shown [10] that these are valid assumptions. It was estimated that possible errors in the heat transfer measurements due to lateral and longitudinal conduction in the wall plates, radiation to the surroundings, the transient effect of slow changes in wall temperature, and the effect of compressibility in the tunnel flow were small. The only correction required was due to the fact that the thermocouple beads, protruding from the back surface of the porous wall, were in contact with injection air which had not yet reached wall temperature. To establish this correction, an extra experiment was performed with blowing but without flow in the tunnel. Extra thermocouples were temporarily installed on the smooth external surface of the porous wall, and their readings were compared with those of the thermocouples on the back surface of the wall. Heat lamps were used as an external heat source for the wall (replacing the usual tunnel flow), and the correction was determined as an empirical function of blowing velocity. At the time that this experiment was performed, it was deemed sufficient to determine the correction as an average over the ten thermocouples in the eighth injection chamber. As it turned out, much of the scatter in the reported Stanton number data may be due to individual variations in the proper value of the correction for each thermocouple. If time had been available to determine the correction individually for each thermocouple, the scatter would probably have been reduced considerably. Equation (3) illustrates the reason why small errors in the wall temperature measurements produce noticeable scatter in the Stanton numbers. It can be seen that measurement of a low value of St depends on the measurement of a small temperature difference, $(T_w - T_c)$.

Qualification of the apparatus

Several tests were carried out to make sure that the tunnel flow was of high enough quality to yield meaningful experimental results. As was mentioned earlier, extensive mass flow surveys showed that the blowing velocity was uniform to within ± 6 per cent. A hot wire probe was used to determine that the root mean square turbulent intensity, $\langle u'^2\rangle^{\frac{1}{2}}/U$, in the free-stream was 0·0025 in the constant pressure section, increasing to 0·0038 near separation. The absence of gross deviations from two-dimensionality was determined by a combination of yaw measurements and measurements

to determine the transverse uniformity of the free-stream velocity. The yaw measurements were made at a distance of $\frac{1}{2}$ in. from the test wall, which was well within the test wall boundary layer. The measurements covered a region extending from the upstream end of the constant pressure section to within 6 in. of the separation point and extending 6 in. to each side of the tunnel centerline. No yaw angles greater than 1 degree were detected. Surveys were also made with two identical static pressure tubes which were traversed simultaneously 6 in. to each side of the tunnel centerline to determine whether there was any transverse variation in free-stream velocity. No variations larger than 1 per cent of the local free-stream velocity were observed. These measurements, along with the observed straightness of the separation line, showed that no gross deviations from two-dimensionality were present. The mean velocity profile results later showed that all of the pressure gradient cases contained small amounts of mean flow convergence. Because of the side wall jets, this convergence was somewhat less than that typically encountered by other investigators of separating flows. Such weak secondary flows do not reduce the value of the data as a test for prediction methods because many methods have provisions for dealing with secondary flow.

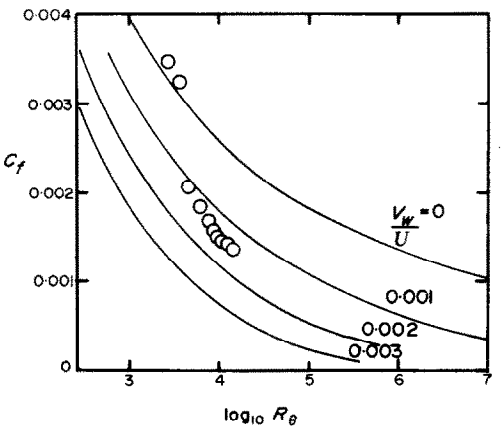

FIG. 3. Comparison of the data for constant pressure, $v_w/U = 0{\cdot}0015$, with Stevenson's prediction. The uppermost two points are upstream of the blown section, and the remaining points are seen to fall between the curves for $v_w/U = 0{\cdot}001$ and 0·002.

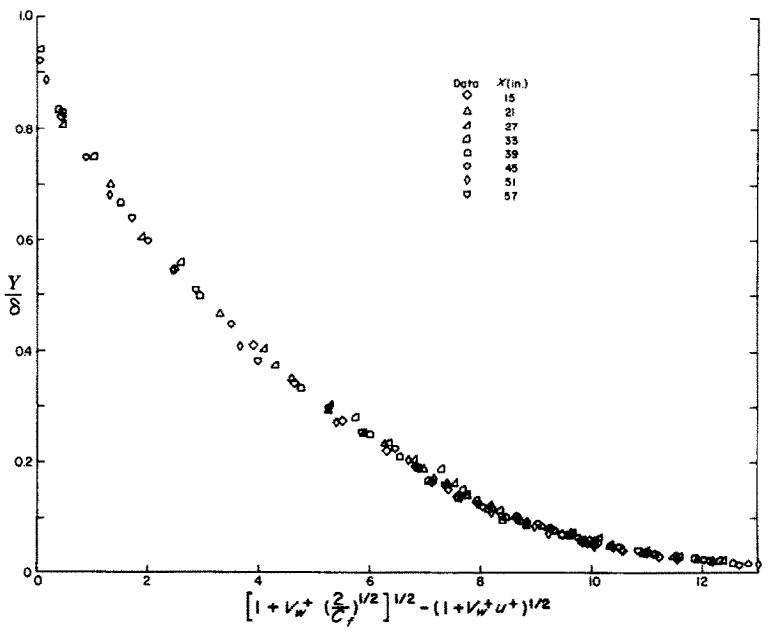

FIG. 4. Stevenson's velocity defect law for constant pressure, $v_w/U = 0{\cdot}0015$.

DISCUSSION OF RESULTS

Constant pressure cases

Mean velocity profile measurements were made for two flows at constant pressure: one without blowing, and one with a blowing rate $v_w/U = 0{\cdot}0015$. In the case without blowing, the velocity profile shapes, the dependence of the skin friction on the Reynolds Number R_θ, and

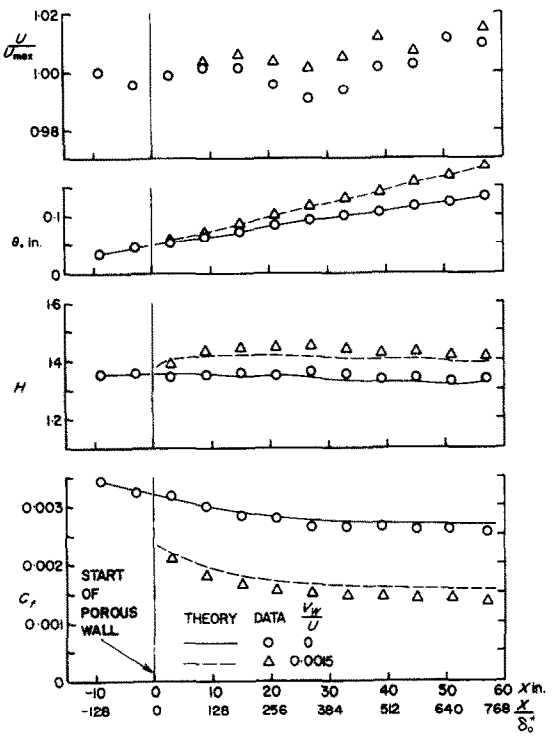

tions of the eddy viscosity model for the constant pressure cases.

the distribution of C_f as a function of X were all in agreement with classical constant pressure results. This gave some assurance that the porous wall was performing as an aerodynamically smooth surface. The data for the case with blowing are also in agreement with the results of other investigators. Figure 3 shows that the skin friction as a function of Reynolds Number agrees well with the relation derived by Stevenson [7]. Figure 4 demonstrates the similarity of the velocity defect profiles in accordance with Stevenson's [7] velocity defect formulation. Figure 5 summarizes the momentum thickness, shape factor, and skin friction results for the constant pressure cases. The increase in momentum thickness and decrease in skin friction caused by transpiration can be seen clearly here.

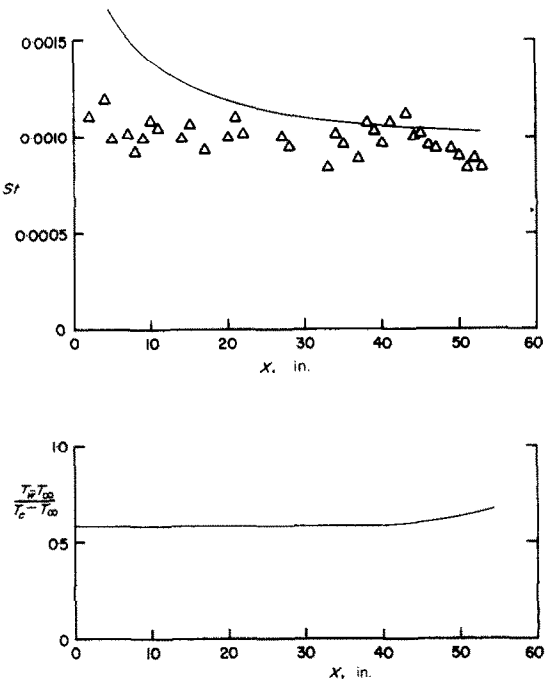

FIG. 6. Experimental Stanton numbers and smoothed wall temperature distribution for constant pressure, $v_w/U = 0{\cdot}0015$.

Figure 6 shows the wall temperature and Stanton Number for the case with blowing. In this case, the injection air was supplied at an initial temperature which was constant with X, and, as a result, the wall temperature varied slightly with X. Since the usual Reynolds analogy for constant pressure flows with nearly constant wall temperature has been found to remain valid with blowing (see Whitten [5]), we would expect the Stanton Number in this case to be slightly greater than $C_f/2$. Comparing the Stanton Number results with the skin friction results of Fig. 5 shows this to be the case.

Pressure gradient cases

The pressure gradient experiments with separation involved two basic flow situations.

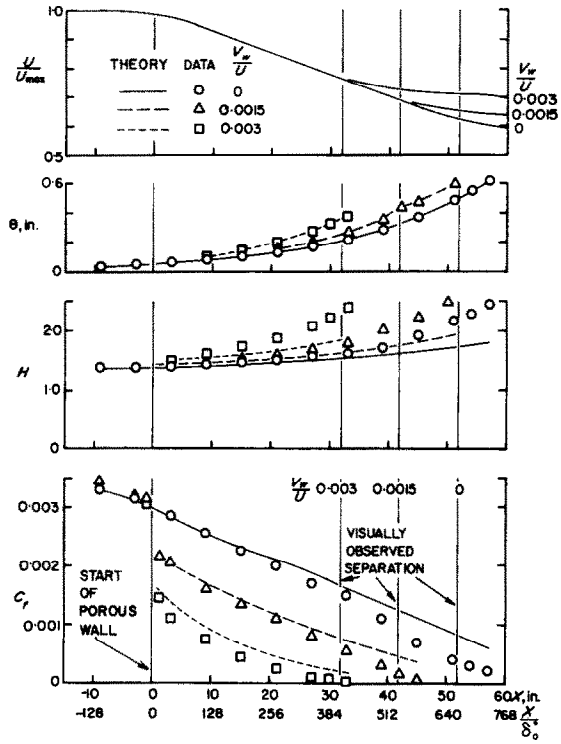

FIG. 7. Principal boundary layer variables and the predictions of the eddy viscosity model for the thin boundary layer cases.

In order to create two flows which differed widely in terms of the relative strength of the pressure gradient, the tunnel was operated in the "thick boundary layer" and "thin boundary layer" configurations discussed earlier. The same free-stream velocity distribution was used in both flows, but because the boundary thicknesses were different, this same pressure gradient was made to look relatively strong in one case and relatively moderate in the other.† The thick boundary layer case resulted in a flow which changed rapidly in response to the pressure gradient, progressing to separation within a relatively small number of boundary layer thicknesses. In the thin boundary layer case, the flow remained attached for a much larger number of boundary thicknesses, and thus this flow corresponds to a milder pressure gradient.

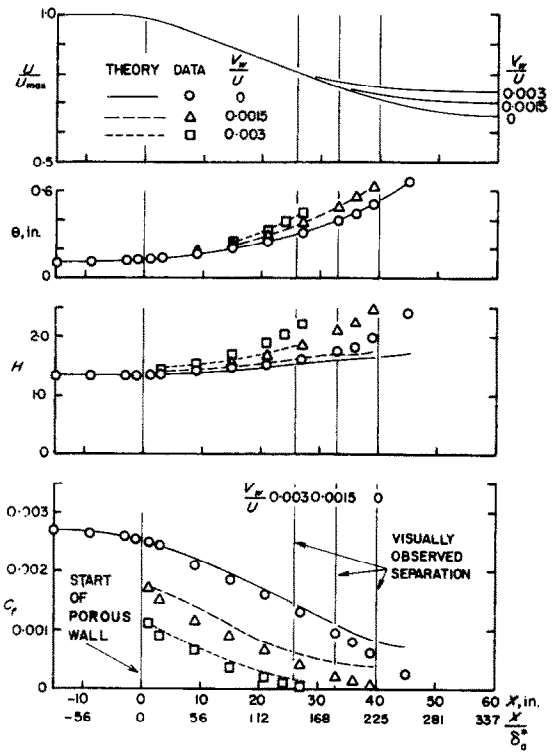

FIG. 8. Principal boundary layer variables and the predictions of the eddy viscosity model for the thick boundary layer cases.

The free-stream velocity distribution used in both cases consisted of a short transition from constant pressure followed by a linear segment which persisted up to the separation point. The blowing velocity distribution was chosen so that the blowing velocity ratio, v_w/U was constant with X upstream of separation. For each of the initial conditions, experiments were

† A parameter which describes the local "strength" of the pressure gradient is $(\delta^*/U)(\partial U/\partial X)$. In the case of equilibrium boundary layers this may be related to the Clauser parameter $(\delta^*/\tau_0)(\partial p/\mathrm{d}x)$ for a specific Reynolds number.

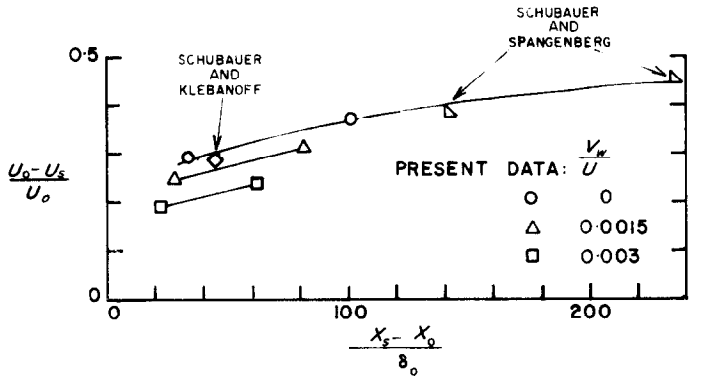

FIG. 9. Relative change in free-stream velocity attained at separation versus the distance in which the flow is brought to separation.

performed with blowing velocity ratios of 0·0, 0·0015 and 0·0030. Figures 7 and 8 show the free-stream velocity distribution and summarize the experimental results for H, θ and C_f. The separation point locations shown were determined by the vane device described earlier. It is clear that the separation point moved upstream as the blowing velocity increased and that the thick boundary layer cases separated sooner than the corresponding thin boundary layer cases.

Figures 9 and 10 present an overall view of the effects of pressure gradient strength and blowing velocity on the separation behavior of these flows. Figure 9 shows how the suddenness with which a flow is brought to separation affects the change in free-stream velocity which can be achieved before separation occurs. The free-stream velocity change, presented non-dimensionally, is plotted against the distance from the start of the pressure rise to the separation point, normalized by the initial boundary layer thickness. The present data for no blowing and data from other investigators [11, 12] who used linear free-stream velocity distributions fall very nearly on a single curve. The slope of the curve illustrates the fact that the more suddenly a flow is brought to separation, the smaller will be the velocity change which can be achieved. Figure 10 shows that for constant blowing velocity ratios, v_w/U, the effect of blowing velocity can be correlated independently of the pressure gradient strength. Here, the free-stream velocity change, normalized by the change which would have occurred without blowing, is seen to fall on a single curve as a function of blowing velocity ratio.

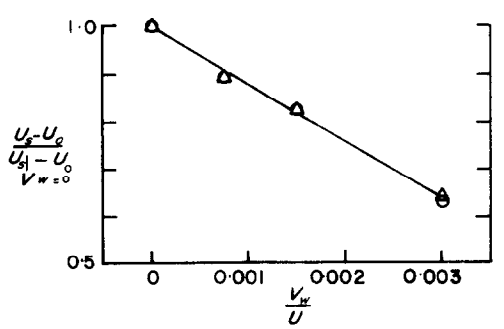

FIG. 10. The effect of blowing velocity on the relative change in free-stream velocity attained at separation.

Stanton Number data for the thick boundary layer case and the thin boundary layer case were substantially the same. Figure 11 shows wall temperatures and Stanton numbers for the thick boundary layer case. The reduction of the Stanton Number due to the pressure gradient is not large, and the deviation from the Reynolds analogy is quite marked.

Predictions of eddy viscosity models

In recent years the availability of high speed digital computers has led to the development of turbulent boundary layer prediction methods based on numerical solution of the boundary layer differential equation of mean motion. All

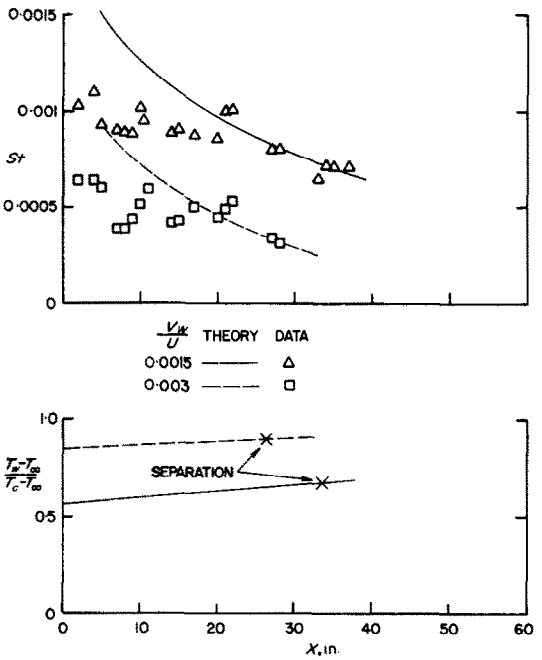

FIG. 11. Experimental Stanton numbers and smoothed wall temperature distributions for the thick boundary layer cases.

such methods depend on empirical hypotheses of one kind or another to characterize the shear stress term in the equation. In an important class of such methods, the shear stress is characterized in terms of an empirical effective viscosity function which depends on the mean flow field. Methods based on this general approach (mean velocity field closure) can differ considerably in detail, but Mellor and Herring [13] have shown that the basic physical content of many of these methods is essentially the same. Thus, the conclusions drawn here are applicable to several of the mean velocity field closure methods now available.

The numerical scheme and effective viscosity hypothesis used here have been described fully in [14–16]. Although the flows involved in our experiments were essentially incompressible, the compressible flow version of the method was used here so that heat transfer could be included in the calculations. The method requires that an initial boundary layer mean velocity profile, temperature profile, and the streamwise distribution of free-stream velocity be specified as initial and boundary conditions. The computer program then proceeds to calculate velocity and temperature profiles at succeeding downstream stations.

Although secondary flow did not appear to be large,† in principle it should be taken into account in making comparisons between theory and data. The prediction method used here has a provision for dealing with convergence or divergence from a plane of symmetry, that is, for dealing with quasi two-dimensional flows in which there is a longitudinal plane in which $w = 0$, but in which $\partial w/\partial z \neq 0$. For this feature of the program to be used, $\partial w_\infty/\partial z$ must be known from the data and supplied as a boundary condition. This leads to difficulty because the uncertainty of our yaw probe measurements did not allow this boundary condition to be supplied with sufficient accuracy. A simpler procedure consists of allowing $\partial w_\infty/\partial z$ to vary so that the calculation duplicates the experimental momentum thickness. In practice this is most easily done by simply "overwriting" θ in the calculation program with the experimental θ. Mellor [14] has found that this procedure gives results nearly identical with those of the full calculation, provided that $\partial w/\partial z$ is not large.

Some typical velocity profiles, along with the corresponding predictions, are shown in Figs.

† Values of θ calculated from the von Karman momentum integral equation using the experimental values of C_f and H were compared with the experimental values. In one case ($v_w = 0$, thick initial boundary layer) the final calculated value of θ at separation was low by 20 per cent. In the other cases, the difference was closer to 10 per cent.

12 and 13. The predictions in the constant pressure cases are quite good, confirming the idea that blowing is not the source of the difficulty in the pressure gradient predictions. In the pressure gradient case shown in Fig. 13, the prediction at $X = 9$ in. is reasonably good, but the prediction at $X = 27$ in. (the last station before separation) shows the error which was already observed in the prediction of H.

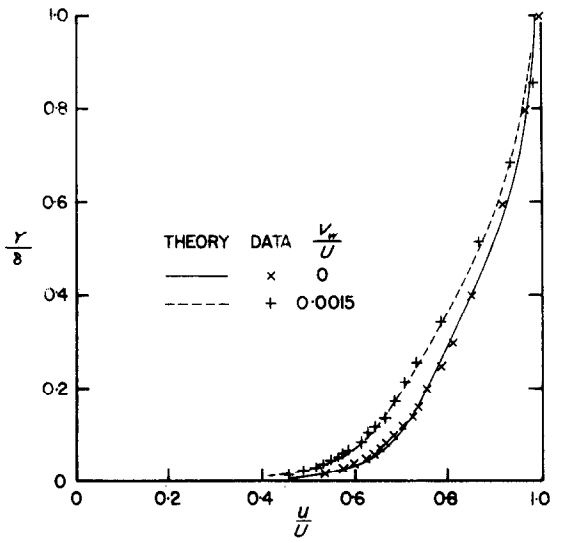

FIG. 12. Predicted and measured velocity profiles at constant pressure, $X = 39$ in., showing the effect of blowing on the constant pressure profiles.

Whether or not the error can be attributed to some kind of turbulence lag is unknown. Because it depends on the local mean flow profile, the effective viscosity cannot model turbulence lag effects. Another possible reason for this difficulty is the fact that the effective viscosity hypothesis does not account for the intermittency of the turbulence in the outer region of the layer. Cebesi and Smith [17] attempted to model the outer region more realistically by including an intermittency factor in their effective viscosity hypothesis, which was otherwise substantially similar to Mellor's. However, the prediction method based on their hypothesis displays the same type of error in adverse pressure gradient flows as does Mellor's method.

In order to evaluate the performance of the hypothesis in the region near the wall in adverse pressure gradients it was necessary to generate a set of predictions which would be independent of the prediction of the outer region. To this end, the simplified equation of motion for the wall region:

$$\frac{\tau}{\rho} = \frac{\tau_w}{\rho} + uv_w + \frac{1}{\rho}\frac{dp}{dx}y \tag{4}$$

was solved numerically to generate families of wall region velocity profiles which could be

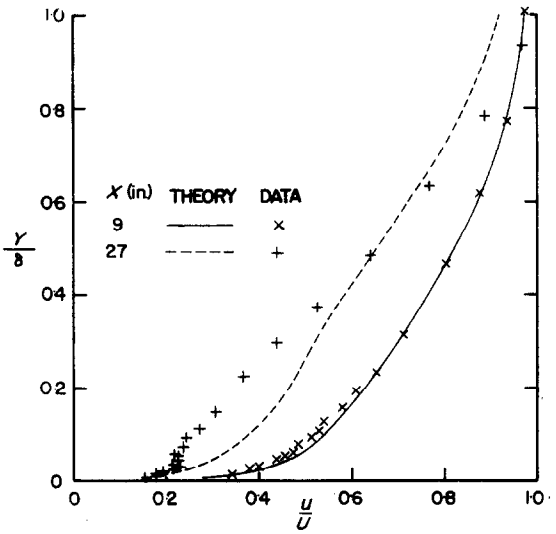

FIG. 13. Predicted and measured velocity profiles for the thick boundary layer case with pressure gradient and $v_w/U = 0{\cdot}0030$, showing the development of the layer toward separation.

compared with the inner regions of the experimental profiles. When $dp/dx = 0$, the solution of this equation in the fully turbulent wall region is the well known logarithmic law of the wall. When $dp/dx \neq 0$, the effective viscosity hypothesis predicts a deviation from the logarithmic profile. The strength of the deviation depends on the magnitude of the pressure gradient parameter $\alpha = \nu(dp/dx)/\rho u^3_\tau$. For comparison with

any particular experimental profile, a family of solutions was generated in which C_f and α were varied so that dp/dx remained constant at the particular experimental value. One of these families and the corresponding experimental data for a typical station near separation are shown in Fig. 14. Lines representing the logarithmic law of the wall for the same values of C_f are included for comparison. The inner region

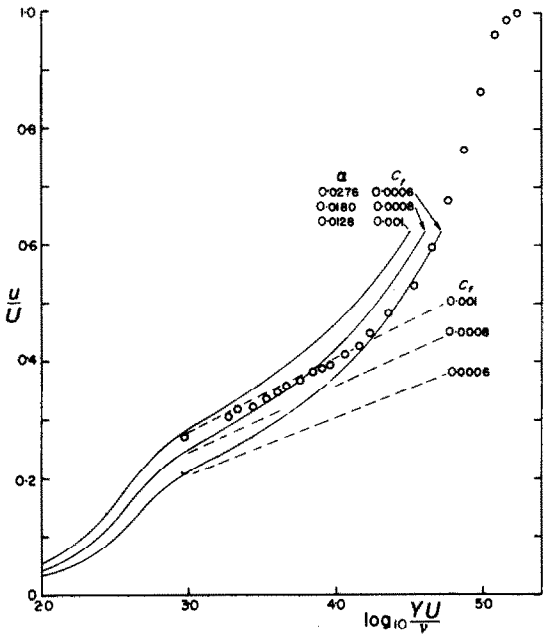

FIG. 14. Velocity profile for the thick boundary layer case without blowing at $X = 33$ in. The solid curves are wall region velocity profiles predicted by the eddy viscosity model, and the dotted lines represent the usual law of the wall.

of the experimental profile definitely appears logarithmic and does not display the deviation predicted by the hypothesis. All of the profiles measured in the program, including those nearest separation, contained apparently logarithmic regions (in Stevenson's form for the cases with blowing), but it is not at all clear why the profiles should have remained logarithmic for such large values of α. Although the profiles appear logarithmic, however, it seems clear that the values of C_f inferred from the law of the wall should be used with caution in the neighbourhood of separation. In the future, experimental innovation will be required to obtain more accurate information about the flow near the wall at high values of α.

The heat transfer portion of the prediction program required the experimental wall temperature as a boundary condition. To provide this in a way suitable to the numerical scheme, smooth curves were drawn through the experimental data. These curves are shown in Figs. 6 and 11, along with the corresponding predictions for the Stanton Number. In view of the scatter of the experimental data, the predictions can be said to agree reasonably well. The fact that the predictions are consistently too high near the start of the blowing is somewhat of a mystery. Experimental error cannot account for the discrepancy. The only explanation which seems plausible at this stage is that the error is due to the fact that the boundary layer energy equation neglects streamwise eddy conduction, which could become important in the present case of a nearly stepwise change in wall temperature.

The law of the wake

The law of the wake, developed by Coles [18], has been shown to represent a good approximation of turbulent boundary layer mean velocity profiles in the impermeable wall case. Because it is applicable to a wide range of pressure distributions, the law of the wake has been used as an important constituent in several integral methods of boundary layer prediction, as in the method developed by Nash and Hicks [19].

It will be verified here that Stevenson's law of the wall yields a form of the law of the wake law which remains valid in pressure gradients and which includes the effects of blowing. The result is simply the formal combination of Stevenson's law of the wall and the wake law, and no added empiricism is necessary. This seems preferable to the law proposed by Black and Sarnecki [1], whose "bilogarithmic" form of the law of the wall with blowing led to a wake

law which required some additional adjustment of the velocity scale in order to fit the data.

The law of the wake with blowing, using Stevenson's law of the wall is:

$$\frac{2}{v_w^+}(1 + v_w^+ u^+)^{\frac{1}{2}} - 1 = \frac{1}{\kappa}\ln y^+ + D + \frac{\pi(X)}{\kappa} W\left(\frac{y}{\delta}\right) \quad (5)$$

where W is a universal function of y/δ. Note that as $v_w^+ \to 0$, the left-hand side approaches u^+, in agreement with the conventional law of the wake.

One difficulty in using equation (5) or in comparing it with experimental data is posed by the problem of defining δ precisely for an experimental profile. For meeting this difficulty, Coles [18] proposed a scheme whereby some known integral property of the experimental profile and the experimental value of C_f are combined with the known properties of the function W to determine π and δ algebraically. In the impermeable wall case, the law of the wake can be combined with the definition of δ^* to give two expressions which can be solved sequentially for π and δ. The law of the wake with blowing yields an analogous pair of equations where δ^* is replaced by an analogous integral thickness, δ'. For the case with blowing, these equations are:

$$2\pi - \ln(1 + \pi) = \kappa \frac{2}{v_w^+}(1 + v_w^+ u^+)^{\frac{1}{2}} - 1 - \ln\frac{\delta' U}{\nu} - \kappa D - \ln\kappa \quad (6)$$

$$\kappa\frac{\delta'}{\delta}\left(\frac{2}{C_f}\right)^{\frac{1}{2}} = 1 + \pi \quad (7)$$

where

$$\delta' = \frac{2}{v_w^+}\int_0^\infty \left(\frac{C_f}{2} + \frac{v_w}{U}\right)^{\frac{1}{2}} - \left(\frac{C_f}{2} + \frac{v_w u}{U^2}\right)^{\frac{1}{2}} dy. \quad (8)$$

As $v_w \to 0$, δ' reduces to δ^*, and equations (6) and (7) reduce to the equations obtained by Coles. These expressions provide a consistent determination of δ which does not depend on a subjective examination of the experimental profiles.

The law of the wake for the impermeable wall case is generally expressed in the form of a velocity profile in which the velocity is written as the sum of a wall region component and a wake region component:

$$u^+ = \frac{1}{\kappa}\ln y^+ + D + \frac{\pi(X)}{\kappa} W\left(\frac{y}{\delta}\right)$$

it is useful to rewrite the law of the wake with blowing in this same form. The result is:

$$u^+ = \mathscr{L}(y^+, v_w^+) + \mathscr{W}\left(v_w^+, y^+, \pi, \frac{y}{\delta}\right)$$

where

$$\mathscr{L} = \frac{v_w^+}{4}\left\{\frac{1}{\kappa}\ln y^+ + D\right\}^2 + \frac{1}{\kappa}\ln y^+ + D$$

and

$$\mathscr{W} = \frac{v_w^+}{4}\left[\frac{\pi}{\kappa} W\left(\frac{y}{\delta}\right)\right]^2 + \left[\frac{v_w^+}{4}\left(\frac{1}{\kappa}\ln y^+ + D\right) + 1\right]\frac{\pi}{\kappa} W\left(\frac{y}{\delta}\right).$$

This profile and its components $\mathscr{L}$ and $\mathscr{W}$ are shown in Fig. 15 for a typical station near separation with blowing. The corresponding experimental data are included for comparison. The agreement is seen to be quite good. It is also interesting to note that the wake component has qualitatively the same shape as Coles' function $W(y/\delta)$. For purposes of comparison, $W(y/\delta)$ was re-normalized so as to have the same amplitude as $\mathscr{W}$ for this particular case and was plotted as the dotted curve in Fig. 15.

A more demanding test of the wake hypothesis is to use the experimental data and the expression for the law of the wake to define an experimentally determined function $W(y/\delta)$ which can be compared with Coles' universal

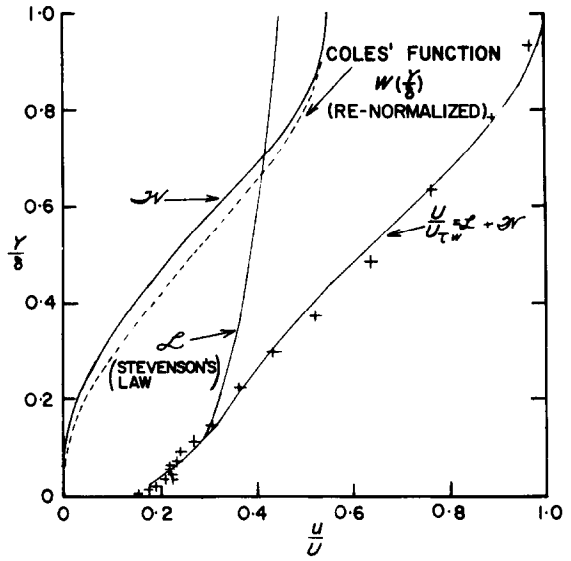

FIG. 15. Plot showing the law of the wake velocity profile and its wall region and wake region components corresponding to the experimental data for the thick boundary layer case with $v_w/U = 0{\cdot}0030$, $X = 27$ in.

CONCLUDING REMARKS

The experimental data presented here† provide an overview of the effect of transpiration on the turbulent boundary layer in an adverse pressure gradient. The gross flow field effects brought about by blowing can be listed as follows: (1) altered velocity profile shapes, (2) lower values of skin friction and Stanton Number, (3) more rapid growth of momentum thickness, and (4) more rapid approach to separation.

The effect of transpiration on separation was found to be substantial. Small blowing rates produced sizable changes in the location of the separation point, accompanied by corresponding reductions in the total change in free-stream velocity which could be achieved before separation. For flows with linear free-stream velocity distributions and constant v_w/U, a correlation was found which relates the total free-stream velocity change to the blowing velocity ratio v_w/U.

The effects of blowing can be predicted accurately by currently available eddy viscosity

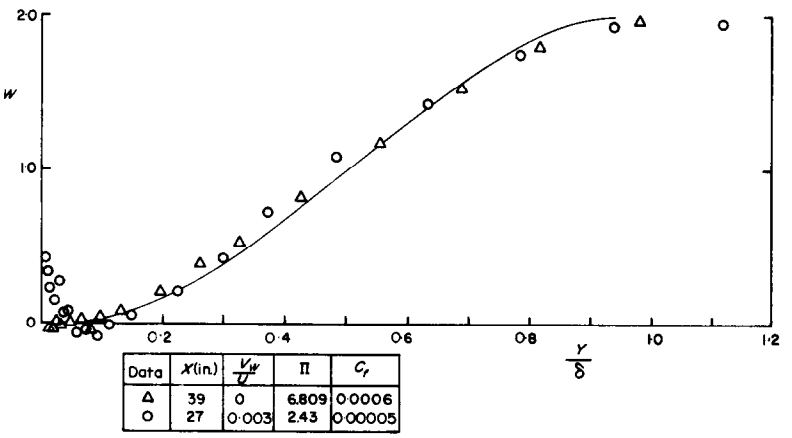

Data	x(in.)	$\frac{v_w}{U}$	Π	C_f
Δ	39	0	6.809	0·0006
o	27	0·003	2.43	0·00005

FIG. 16. Wake components near separation for the thick boundary layer case with and without blowing.

function. This was done for all of the profiles in the experimental program, and the agreement was good except in a short region immediately downstream of the start of the blowing. Figure 16 shows a comparison between the experimental $W(y/\delta)$ and Coles' function for typical cases near separation with and without blowing.

† In the interest of clarity, only a few velocity profiles were presented in this paper. Complete tables of the velocity profile data are available, on request, from the authors.

prediction methods. In separating flows, eddy viscosity methods can predict skin friction and Stanton Number with sufficient accuracy for many engineering purposes. Inaccuracies in the prediction of velocity profile shapes in flows approaching separation appeared to be a result of the strong pressure gradient and seemed to be independent of the presence or absence of blowing.

The law of the wake was found to provide a good representation of velocity profiles in the presence of blowing, except in the vicinity of step changes in blowing rate. This representation could provide the basis for an integral method of predicting flows with transpiration.

REFERENCES

1. T. J. BLACK and A. J. SARNECKI. The turbulent boundary layer with suction or injection. Cambridge University Engineering Department, Reports and Memoranda No. 3387 (1958).
2. T. N. STEVENSON. Experiments on injection into an incompressible turbulent boundary layer. The College of Aeronautics, Cranfield, Report Aero No. 177 (1964).
3. J. MCQUAID. Experiments on incompressible turbulent boundary layers with distributed injection. Great Britain, Aeronautical Research Council. A.R.C. **28**. 735 (1967).
4. R. L. SIMPSON, W. M. KAYS and R. J. MOFFAT. The turbulent boundary layer on a porous plate: An experimental study of the fluid dynamics with injection and suction. Stanford University, Department of Mechanical Engineering, Thermosciences Division. Report No. HMT-2 (1967).
5. D. G. WHITTEN, W. M. KAYS and R. J. MOFFAT. The turbulent boundary layer on a porous plate: Experimental heat transfer with variable suction, blowing and surface temperature. Stanford University, Department of Mechanical Engineering, Thermosciences Division. Report No. HMT-3 (1967).
6. T. N. STEVENSON. A law of the wall for turbulent boundary layers with suction or injection. The College of Aeronautics, Cranfield, Report No. 166 (1963).
7. T. N. STEVENSON. A modified defect law for turbulent boundary layers with injection. The College of Aeronautics, Cranfield, Report Aero No. 170 (1963).
8. R. J. LOYD, R. J. MOFFAT and W. M. KAYS. The turbulent boundary layer on a porous plate: An experimental study of the fluid dynamics with strong favorable pressure gradients and blowing. Stanford University, Department of Mechanical Engineering, Thermosciences Division. Report No. HMT-13 (1970).
9. D. W. KEARNEY, R. J. MOFFAT and W. M. KAYS. The turbulent boundary layer: Experimental heat transfer with strong favorable pressure gradients and blowing. Stanford University, Department of Mechanical Engineering, Thermosciences Division, Report No. HMT-12 (1970).
10. J. D. MCLEAN. The transpired turbulent boundary layer in an adverse pressure gradient. Princeton University, Department of Aerospace and Mechanical Sciences. Ph.D. Thesis (1970).
11. G. B. SCHUBAUER and P. S. KLEBANOFF. Investigation of separation of the turbulent boundary layer. NACA TN-2133 (1950).
12. G. B. SCHUBAUER and W. G. SPANGENBERG. Forced mixing in boundary layers. *J. Fluid Mech.* **8**. 1–32 (1960).
13. G. L. MELLOR and H. J. HERRING. A study of turbulent boundary layer models; Part I. mean velocity field closure. Princeton University, AMS Report No. 914 (May 1970).
14. G. L. MELLOR. Turbulent boundary layers with arbitrary pressure gradients and divergent or convergent cross flows. *AIAA Jl* **5**. 1570–1579 (1967).
15. H. J. HERRING and G. L. MELLOR. A method of calculating compressible turbulent boundary layers. NASA Contractor Report, CR-1144 (1968).
16. H. J. HERRING and G. L. MELLOR. A computer program to calculate incompressible laminar and turbulent boundary layer development. NASA CR-1564 (1970).
17. J. CEBECI and A. M. O. SMITH. A finite difference solution of the incompressible turbulent boundary layer equations by an eddy-viscosity concept. Proceedings, Computation of Turbulent Boundary Layers, AFOSR-IFP Stanford Conference. Vol. 1 (1968).
18. D. E. COLES. The law of the wake in the turbulent boundary layer. *J. Fluid Mech.* **1**. 191–226 (1956).
19. J. F. NASH and J. G. HICKS. An integral method including the effect of upstream history on the turbulent shear stress. Proceedings, Computation of Turbulent Boundary Layers. AFOSR-IFP Stanford Conference. Vol. 1 (1968).

COUCHE LIMITE TURBULENTE AVEC TRANSPIRATION DANS UN GRADIENT DE PRESSION ADVERSE

Résumé—Un programme expérimental a été conduit pour étudier l'effet de la transpiration sur une couche limite turbulente dans un gradient de pression adverse. Une soufflerie avec une paroi poreuse a été conçue de telle sorte que la vitesse de soufflage et l'intensité du gradient de pression puissent être modifiées au cours des expériences. On a étudié l'effet de la transpiration sur l'emplacement du point de séparation. Des mesures de profils de vitesse moyenne et de flux thermiques ont été comparées aux estimations d'une

méthode de calcul de couche limite basée sur un modèle à viscosité effective. Des estimations de frottement pariétal sont satisfaisantes, mais il y a une erreur notable dans les formes du profil de vitesse prédites près de la séparation. On a aussi trouvé qu'une forme de la loi de sillage fournit une bonne représentation des profils de vitesse avec soufflage et qu'elle peut être utilisée comme base d'une méthode intégrale de calcul.

DIE TURBULENTE GRENZSCHICHT MIT AUSBLASUNG BEI ANSTEIGENDEM DRUCKGRADIENTEN

Zusammenfassung—Es wurde ein experimentelles Program ausgearbeitet, um die Auswirkungen der Ausblasung auf eine turbulente Grenzschicht bei ansteigendem Druckgradienten zu ermitteln. Es wurde ein Windkanal mit einer porösen Wand so gebaut, dass die Blasgeschwindigkeit und die Grösse des Druckgradienten im Verlaufe der Versuche verändert werden konnten. Die Auswirkung des Ausblasens auf die Position des Ablösungspunktes wurde beobachtet. Die Messungen des Geschwindigkeitsprofils und des Wärmeüberganges werden verglichen mit Voraussagen aufgrund einer Rechenmethode für Grenzschichten mit Hilfe eines Modells der effektiven Zähigkeit. Die Voraussagen für die Wandreibung waren zufriedenstellend. Doch es gab merkliche Fehler gegenüber dem berechneten Geschwindigkeitsprofil in der Nähe der Ablösung. Es wurde ebenso herausgefunden, dass eine Form des Gesetzes für den vollturbulenten Bereich der Grenzschicht ("Nachlaufgesetz") eine gute Wiedergabe des Geschwindigkeitsprofils mit Ausblasen gestatt und dass dies als Grundlage f r eine integrale Rechenmethode dienen kan

ИСПАРЯЮЩИЙСЯ ТУРБУЛЕНТНЫЙ ПОГРАНИЧНЫЙ СЛОЙ ПРИ НАЛИЧИИ ПОЛОЖИТЕЛЬНОГО ГРАДИЕНТА ДАВЛЕНИЯ

Аннотация—Проведено экспериментальное исследование влияния сублимационного испарения на турбулентный пограничный слой при наличии положительного градиента давления. Аэродинамическая труба с пористой стенкой была сконструирована таким образом, чтобы при проведении опытов можно было менять скорость вдува и градиент давления. Было отмечено влияние сублимационного испарения на положение точки отрыва. Измерения профилей средней скорости и интенсивности переноса тепла сравнивались с результатами теоретического расчета пограничного слоя методом, основанном на модели эффективной вязкости. Теоретические расчеты поверхностного трения были удовлетворительными, однако выявилась заметная ошибка в расчетных формах профиля скорости у точки отрыва. Найдено также, что форма закона спутной струи дает хорошее представление о профилях скорости при вдуве и может использоваться как основа для интегрального метода расчета.